Phytochemistry 164 (2019) 122–129

Contents lists available at ScienceDirect

Phytochemistry

journal homepage: www.elsevier.com/locate/phytochem

Isolation of enantiomeric furolactones and furofurans from *Rubus idaeus* L. with neuroprotective activities

Le Zhou[a], Feng-Ying Han[a], Li-Wei Lu[a], Guo-Dong Yao[a], Ying-Ying Zhang[a], Xiao-Bo Wang[b], Bin Lin[c], Xiao-Xiao Huang[a,b,**], Shao-Jiang Song[a,*]

[a] School of Traditional Chinese Materia Medica, Key Laboratory of Computational Chemistry-Based Natural Antitumor Drug Research & Development, Liaoning Province, Shenyang Pharmaceutical University, Shenyang, 110016, China
[b] Chinese People's Liberation Army 210 Hospital, Dalian, 116021, China
[c] School of Pharmaceutical Engineering, Shenyang Pharmaceutical University, Shenyang, 110016, China

ARTICLE INFO

Keywords:
Rubus idaeus
Rosaceae
Lignans
Enantiomeric
DP4 plus
Calculated ECD
Neuroprotective

ABSTRACT

A phytochemical study on the fruits of *Rubus idaeus* L. (Rosaceae) yielded eight pairs of enantiomeric lignans, including one undescribed furolactone named (−)-idaeusinol A and six undescribed furofuran derivatives named (+/−)-idaeusinol B–D. The structures of these isolated compounds were elucidated by spectroscopic analyses and a combination of computational techniques including gauge-independent atomic orbital (GIAO) calculation of 1D NMR data and TD-DFT calculation of electronic circular dichroism (ECD) spectra. Bioactivity screenings suggested that (+)-idaeusinol D exhibited the most significant protective effect against H_2O_2-induced neurotoxicity at the concentration of 25 μM. In contrast, (−)-idaeusinol D, as the enantiomer of (+)-idaeusinol D, showed no effect against H_2O_2-induced neurotoxicity at both 25 and 50 μM concentration.

1. Introduction

Lignans are an important class of naturally occurring metabolites biosynthetically generated from two (or more) units of phenylpropanoid monomers by the free-radical coupling reaction. They are widely spread within the plant kingdom (Teponno et al., 2016). Due to their structural diversity, lignans exhibit multifarious clinical pharmacological activities, such as antitumor (Chen et al., 2013), anti-inflammatory (Kim et al., 2012), calcium antagonistic, antioxidant (Lu et al., 2016; Mei et al., 2009; Min et al., 2004), antiviral (Xue et al., 2015), and antihyperglycemic effects (Kumar et al., 2009). In recent years, owing to their fascinating chemical structures and remarkable biological activities, these compounds have attracted great interest from the synthetic and pharmacological communities. Such naturally occurring lignans normally exist as racemates due to their biosynthetic origin through free-radical coupling reactions. For a long time, they have rarely been analyzed systematically for their enantiomeric purity.

Rubus idaeus L. (raspberry), taxonomically belonging to the family of Rosaceae, is widely distributed in temperate and subtropical areas. Its fresh fruits are edible, and the dried fruits, known as “fu-pen-zi”, have been traditionally used as a folk medicine in China frequently prescribed for the treatment of colic pain, diarrhea, kidney disease and neurodegenerative disorders (Blumenthal, 1998; Garcia et al., 2017; Ghalayini et al., 2011). Previous phytochemical investigations of this species were mainly focused on the characterization of flavonoids and phenolic acids derivatives, including quercetin, rutin, pinoresinol, ellagic acid, caffeic acid (Ciric et al., 2018; Rao and Snyder, 2010). Apart from these phenolic derivatives, *Rubus* species and raspberry also contain other classes of constituents (Mazur et al., 2000; Mcdougall et al., 2017). To identify more bioactive substances responsible for the beneficial effects of *R. idaeus* fruits, further chemical investigation was conducted in this study. As a result, eight pairs of enantiomers (**1a/1b**-**8a/8b**, Fig. 1), including two pairs of enantiomeric furolactones (**1a/1b** and **5a/5b**), four pairs of enantiomeric furofurans (**2a/2b** and **6a/6b**-**8a/8b**), and two pairs of enantiomeric sesquilignans (**3a/3b** and **4a/4b**) were isolated from the fruits of the plant. The enantioseparations of these compounds were achieved using chiral HPLC approach. Their 2D structures and relative configurations were elucidated by extensive spectroscopic analyses. Notably, (±)-idaeusinol A (**1**), a furolactone, its relative configuration was established by employing gauge-including atomic orbitals (GIAO) NMR chemical shift calculations, with the aid of the advanced statistical method DP4 plus (Grimblat et al., 2015). Additionally, their absolute configurations were determined by comparison of experimental and calculated ECD spectra. Their neuroprotective

* Corresponding author.
** Corresponding author. School of Traditional Chinese Materia Medica, Shenyang Pharmaceutical University, Shenyang, 110016, China.
E-mail addresses: xiaoxiao270@163.com (X.-X. Huang), songsj99@163.com (S.-J. Song).

https://doi.org/10.1016/j.phytochem.2019.05.008
Received 14 November 2018; Received in revised form 18 March 2019; Accepted 9 May 2019

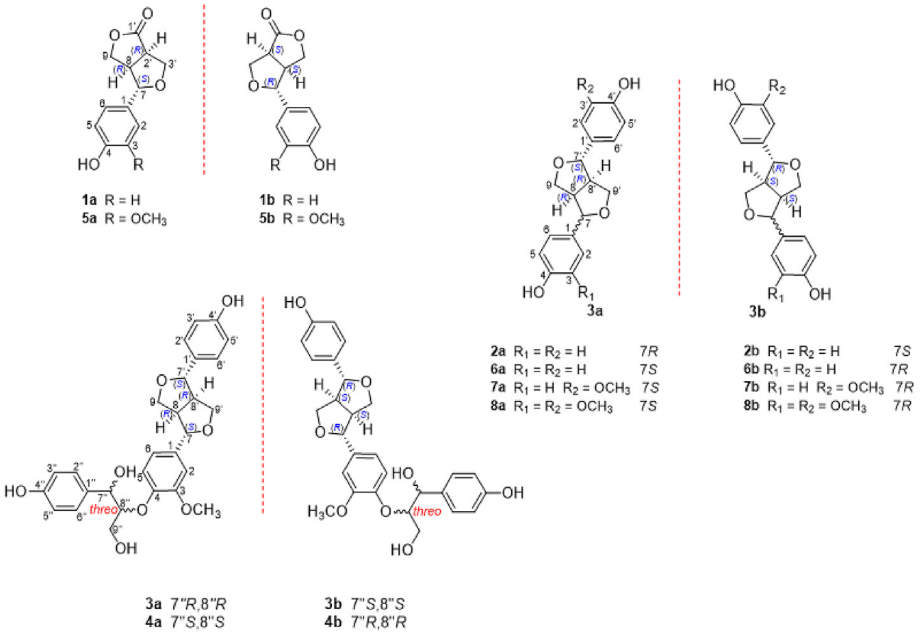

Fig. 1. Chemical structures of compounds **1a/1b–8a/8b**.

effects against H_2O_2-induced oxidative injury in human neuroblastoma SH-SY5Y cells were investigated.

2. Results and discussion

Compound **1** (**1a**/**1b**) was obtained as a pale amorphous gum. Its molecular formula was deduced as $C_{12}H_{12}O_4$, on the pseudo-molecular ion peak at *m/z* 243.0605 $[M + Na]^+$ in the HRESIMS, indicating seven degrees of unsaturation. The presence of a hydroxy and a benzene ring were suggested by the IR spectrum, showing absorptions at 3423, 1630 and 1427 cm^{-1}. The ^1H NMR data (Table 1) showed the signals for a 1,4-disubstituted phenyl ring due to the aromatic proton signals at δ_H 7.20 (2H, d, J = 8.5 Hz, H-2/6) and 6.79 (2H, dd, J = 8.5 Hz, H-3/5). Additionally, the characteristic signals at δ_H 4.64 (1H, d, J = 6.6 Hz, H-7), 4.50 (1H, d, J = 9.6, 6.9 Hz, H-9a), 4.32 (1H, dd, J = 9.6, 2.0 Hz, H-9b), 4.25 (1H, t, J = 8.7 Hz, H-3′a), 4.05 (1H, dd, J = 9.1, 3.4 Hz, H-3′b), 3.52 (1H, td, J = 8.7, 3.4 Hz, H-2′), and 3.16 (1H, dtd, J = 8.9, 6.7, 2.0 Hz, H-8) indicated the existence of a 3,7-dioxabicyclo[3.3.0] octan-2-one skeleton. This deduction was further verified by the HMBC and ^1H–^1H COSY spectra (Fig. 2). The ^1H NMR signal at δ_H 4.64 (H-7) showed correlations with C-1 (δ_C 131.5) and C-2/6 (δ_C 128.8), indicating that the phenyl group was located at C-7 position.

In the NOESY spectrum (Fig. 2), δ_H 3.16 (H-8) showed cross-peaks with δ_H 3.52 (H-2′), 4.50 (H-9a) and 7.21 (H-2/6) indicated the same orientation of these protons. On the other hand, correlation between δ_H 4.26 (H-7) and δ_H 3.52 (H-9b) was used to place them on the opposite face. Moreover, the relative configuration at C-7 was further assigned by employing calculations of shielding tensor values with support from DP4+ probability analysis. The theoretical calculations of ^{13}C NMR data of the two possible isomers (7*S**,8*R**,2′*R**)-**1** and (7*R**,8*R**,2′*R**)-**1** (Fig. 3) were predicted using the GIAO method with the Gaussian 09 software (Frisch et al., 2009) at the B3LYP/6-311 + G(d,p) level utilizing the polarizable continuum model (PCM) in methanol. Comparison of the experimental and calculated ^{13}C NMR data allowed the determination of the relative configuration of **1** as 7*S**,8*R**,2′*R** with a DP4+ probability of approximately 98.4%. The absolute configuration of **1** was determined by comparison of experimental and calculated electronic circular dichroism (ECD). The calculated ECD of 7*S*,8*R*,2′*R*-**1** is consistent with the measured ECD of (+)-**1a** but opposite of that of (−)-**1b** (Fig. 4). Therefore, the structure of (+)-**1a**, namely, (+)-idaeusinol A (Li et al., 2013), was deduced to be (7*S*,8*R*,2′*R*), and (−)-**1b**, namely, (−)-idaeusinol A, was deduced to be (7*R*,8*S*,2′*S*).

Compound **2** (**2a**/**2b**), obtained as a colorless, light oil, was assigned the molecular formula $C_{18}H_{18}O_4$, the same as **6**, based on its sodiated molecular ion at *m/z* 321.1085 $[M + Na]^+$ (calcd 321.1097) in the HRESIMS. Analysis of the NMR data of **2** indicated that it was an isomer of **6**, due to their closely similar spectroscopic features. However, the two symmetric oxymethine signals [δ_H 4.59 (2H, d, J = 4.0 Hz, H-2/6] of the furofuran ring in **6** were split into a higher field signal with smaller coupling constant [δ_H 4.74 (1H, d, J = 5.9 Hz, H-2)] and a lower field signal with larger coupling constant [4.27 (1H, d, J = 7.0 Hz, H-6)] in the ^1H NMR spectrum of **2**. Some of the aliphatic carbon signals were shifted to a higher field [δ_C 81.4 (C-6, $\Delta\delta_C$ −3.3), δ_C 68.8 (C-8, $\Delta\delta_C$ −2.0), δ_C 49.4 (C-1, $\Delta\delta_C$ −4.2)], which was likely due to the anisotropic effect of an aromatic ring. Naturally occurring furofurans have been reported to possess typical *cis*-8,8′-fused (Lu et al., 2015). The chemical shift differences of H_2-9 and H_2-9′ ($\Delta\delta_{H\text{-}9}$ 0.29; $\Delta\delta_{H\text{-}9'}$ 0.62) of 8-H type furofuran lignans indicated 7-H/8-H *trans*, 7′-H/8′-H *cis* relative configurations (Shao et al., 2018). The smaller value of the specific rotation {$[\alpha]^{20}_D$ −0.3 (*c* 0.1, MeOH)} compared with that of its stereoisomer indicated that **2** was likely a partial racemic mixture. Subsequently, the chiral HPLC purification of **2** afforded the enantiomers **2a** and **2b** with opposite specific rotation and mirror imaged Cotton effects in their ECD spectra. The absolute configurations of (−)-**2** and (+)-**2** were determined as (7*R*,8*R*;7′*R*,8′*S*) (**2a**) and (7*S*,8*S*;7′*S*,8′*R*) (**2b**), respectively, by comparison of the experimental and calculated ECD spectra (Fig. 4). Thus, the absolute configuration of (−)-**2a** was elucidated as 7*R*,8*R*;7′*R*,8′*S* and that of (+)-**2b** as 7*S*,8*S*;7′*S*,8′*R*, and the compounds **2a** and **2b** were assigned the names (−)-idaeusinol B and (+)-idaeusinol B, respectively.

Compound **3** (**3a**/**3b**) and **4** (**4a**/**4b**) were obtained as a mixture of light yellow oil and displayed only a single chromatographic peak on the reversed-phase HPLC. However, the carbon signals at δ_C 110.6 and 118.3, which were assigned to δ_H 6.93 (1H, d, J = 1.6 Hz, H-2) and 6.82 (1H, dd, J = 8.4, 1.6 Hz, H-6), respectively, were both split in the ^{13}C NMR spectrum. Subsequently, a series of chiral HPLC resolutions were performed to understand this distinctive discord. The results revealed that the isolate was a mixture of stereoisomers, which afforded two pairs of enantiomers **3a**/**3b** and **4a**/**4b**, corresponding to the four peaks observed from the chiral HPLC (Fig. S19).

Table 1
^{1}H (400 MHz) and ^{13}C (100 MHz) data of enantiomers **1–4** in DMSO-d_6 (δ in ppm).

No.	1[a]		2		3		4	
	δ_H, mult. (J in Hz)	δ_C	δ_H, mult. (J in Hz)	δ_C	δ_H, mult. (J in Hz)	δ_C	δ_H, mult. (J in Hz)	δ_C
1		131.5		128.8		134.4		134.4
2	7.20 (d, J = 8.5 Hz)	128.8	7.13 (d, J = 8.3 Hz)	126.6	6.93 (d, J = 1.6 Hz)	110.6	6.93 (d, J = 1.6 Hz)	110.6
3	6.79 (d, J = 8.5 Hz)	116.3	6.73 (d, J = 8.3 Hz)	115.0		149.7		149.7
4		158.6		156.3		147.9		147.9
5	6.79 (d, J = 8.5 Hz)	116.3	6.73 (d, J = 8.3 Hz)	115.0	6.97 (d, J = 8.4 Hz)	115.7	6.97 (d, J = 8.4 Hz)	115.7
6	7.20 (d, J = 8.5 Hz)	128.8	7.13 (d, J = 8.3 Hz)	126.6	6.82 (dd, J = 8.4, 1.6 Hz)	118.4	6.82 (dd, J = 8.4, 1.6 Hz)	118.4
7	4.64 (d, J = 6.6 Hz)	87.6	4.74 (d, J = 5.9 Hz)	81.4	4.63 (d, J = 4.7 Hz)	85.0	4.63 (d, J = 4.7 Hz)	85.0
8	3.16 (dtd, J = 8.9, 6.6, 2.0 Hz)	49.1	3.30, m	49.4	3.02, overlap	53.5	3.02, overlap	53.5
9	4.50 (dd, J = 9.6, 6.9 Hz)	71.8	3.66 (t, J = 8.6 Hz)	68.8	4.11, overlap	71.0	4.11, overlap	71.0
	4.32 (dd, J = 9.6, 2.0 Hz)		3.04 (t, J = 8.6 Hz)		3.72, overlap		3.72, overlap	
1′		181.1		131.5		131.5		131.5
2′	3.52 (td, J = 8.9, 3.4 Hz)	47.5	7.15 (d, J = 8.6 Hz)	127.4	7.15 (d, J = 8.5 Hz)	127.5	7.15 (d, J = 8.5 Hz)	127.5
3′	4.25 (t, J = 8.7 Hz)	70.8	6.72 (d, J = 8.6 Hz)	114.9	6.73 (d, J = 8.5 Hz)	115.1	6.73 (d, J = 8.5 Hz)	115.1
	4.05 (dd, J = 9.1, 3.4 Hz)							
4′				156.9		156.8		156.8
5′			6.72 (d, J = 8.6 Hz)	114.9	6.73 (d, J = 8.5 Hz)	115.1	6.73 (d, J = 8.5 Hz)	115.1
6′			7.15 (d, J = 8.6 Hz)	127.4	7.15 (d, J = 8.5 Hz)	127.5	7.15 (d, J = 8.5 Hz)	127.5
7′			4.27 (d, J = 7.0 Hz)	86.9	4.61 (d, J = 4.6 Hz)	85.0	4.61 (d, J = 4.6 Hz)	85.0
8′			2.78 (m)	53.9	3.02, overlap	53.7	3.02, overlap	53.7
9′			4.00 (d, J = 9.2 Hz)	70.9	4.11, overlap	71.0	4.11, overlap	71.0
			3.71 (dd, J = 9.2, 6.3 Hz)		3.72, overlap		3.72, overlap	
1″						132.3		132.3
2″/6″					7.17 (d, J = 8.4 Hz)	127.9	7.17 (d, J = 8.4 Hz)	127.9
3″/5″					6.68 (d, J = 8.4 Hz)	114.5	6.68 (d, J = 8.4 Hz)	114.5
4″						156.4		156.4
7″					4.71 (d, J = 4.7 Hz)	70.8	4.71 (d, J = 4.7 Hz)	70.8
8″					4.20, m	85.0	4.20, m	85.0
9″					3.56 (dd, J = 11.5, 3.7 Hz)	60.1	3.56 (dd, J = 11.5, 3.7 Hz)	60.1
					3.22 (dd, J = 11.5, 6.3 Hz)		3.22 (dd, J = 11.5, 6.3 Hz)	
OCH_3					3.77, s	55.8	3.77, s	55.8

[a] Measured in CD_3OD.

The molecular formula of **3** (**3a/3b**) was deduced as $C_{28}H_{30}O_8$ by the HRESIMS ion peak at m/z 517.1854 $[M + Na]^+$ (calcd 517.1838), corresponding to fourteen degrees of unsaturation. The NMR spectrum indicated the presence of a 1,3,4-trisubstituted and two symmetrical 1,4-disubstituted aromatic rings, one aromatic methoxyl, three oxymethylenes, and six methine (four oxygenated) groups. These data suggested that **3** was a sesquineolignan. Moreover, comparison of the NMR data between **3** (Table 1) and (±)-demethoxypinoresinol (**7**) indicated that they differed in the presence of resonances attributable to an additional 4″-hydroxyphenylglycerol-8″-yl moiety in **3**. In the HMBC spectrum (Fig. 2), correlation from H-8″ to C-4 verified the 8″,4-oxy linkage in **3**. On the basis of the similar chemical shift differences of H_2-9 and H_2-9′ ($\Delta\delta_{H\text{-}9}$ 0.39; $\Delta\delta_{H\text{-}9'}$ 0.39) in the 3,7-dioxabicyclo[3.3.0]octane moiety, the partial relative configuration of **3** was established as 7*R**,8*S**,7′*R**,8′*S**, which was identical to that of **7**. The 7″,8″-*threo* configuration was elucidated by the larger coupling constant between H-7″ and H-8" ($J_{7'',8''}$ = 8.2 Hz in $CDCl_3$) (Xiong et al., 2011). The absolute (7*S*,8*R*;7′*S*,8′*R*;7″*R*,8″*R*)-configuration of **3a** was determined by

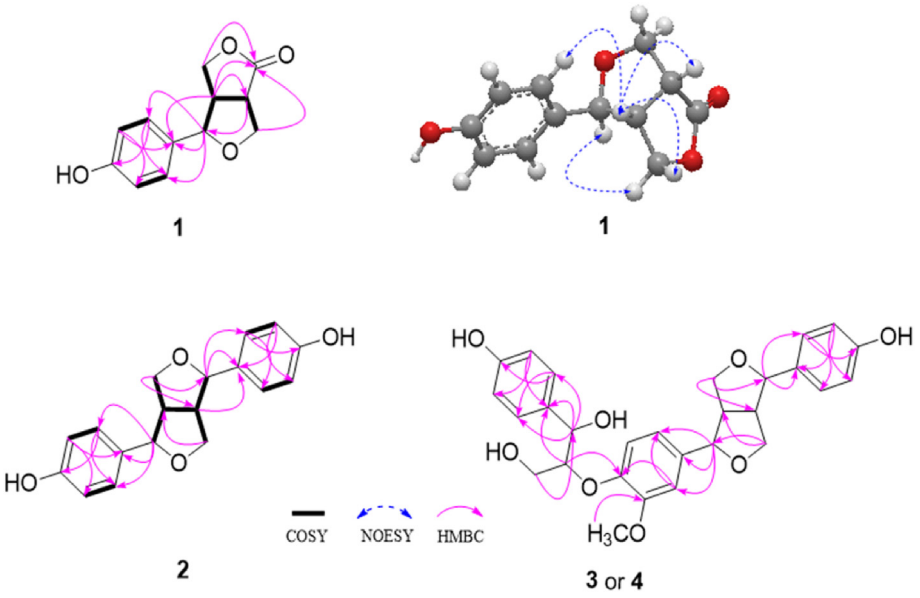

Fig. 2. Selected ^{1}H–^{1}H COSY, HMBC and NOESY correlations of compounds **1–4**.

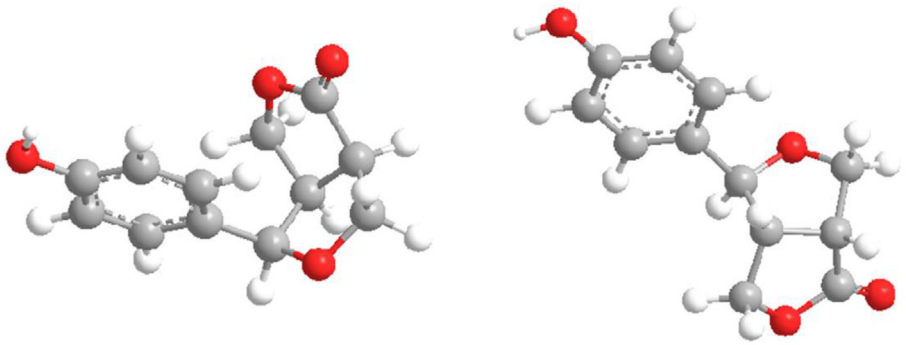

Fig. 3. Two plausible diastereomers of **1** used for the DP4+ application.

comparison of its experimental and computed ECD curves (Fig. 4). Thereby, the absolute configuration of **3a** and **3b** were determined as (7*S*,8*R*;7′*S*,8′*R*;7″*R*,8″*R*) and (7*R*,8*S*;7′*R*,8′*S*;7″*S*,8″*S*) with the trivial names of (+)-idaeusinol C and (−)-idaeusinol C, respectively.

Compound **4** (**4a**/**4b**) had the same molecular formula, $C_{28}H_{30}O_8$, as that of **3**. Compounds **3** and **4** were suggested by their identical NMR spectra to have the same planar structure and relative configurations. Detailed comparison of the experimental ECD data between **3a** and **4a** (or **3b** and **4b**) indicated that there were obvious differences at the region of 200–225 nm in their experimental ECD curves (Fig. S34). The absolute configurations of **4a** and **4b** were designated as (7*S*,8*R*;7′*S*,8′*R*;7″*S*,8″*S*) and (7*R*,8*S*;7′*R*,8′*S*;7″*R*,8″*R*) by comparison of the experimental and theoretical ECD. Thus, the absolute configurations of **4a** and **4b** were assigned as (7*S*,8*R*;7′*S*,8′*R*;7″*S*,8″*S*) and (7*R*,8*S*;7′*R*,8′*S*;7″*R*,8″*R*) with the trivial names of (+)-idaeusinol D and (−)-idaeusinol D, respectively.

The known compounds were identified via comparison of their spectroscopic data with literature values as (+)-salicifoliol (**5a**) (Yamauchi et al., 2004), (−)-salicifoliol (**5b**) (González et al., 1989), (+)-ligballinol (**6a**) (Kobayayashi and Ohta, 1983), (−)-ligballinol (**6b**) (Wang et al., 2009), (+)-demethoxypinoresinol (**7a**) (Cuenca et al., 1991), (−)-demethoxypinoresinol (**7b**) (Hosokawa et al., 2004), (+)-pinoresinol (**8a**) (Cuenca et al., 1991), (−)-pinoresinol (**8b**) (Li et al., 2012).

2.1. Neuroprotective activity

Lignans are a large group of naturally occurring phenols with great

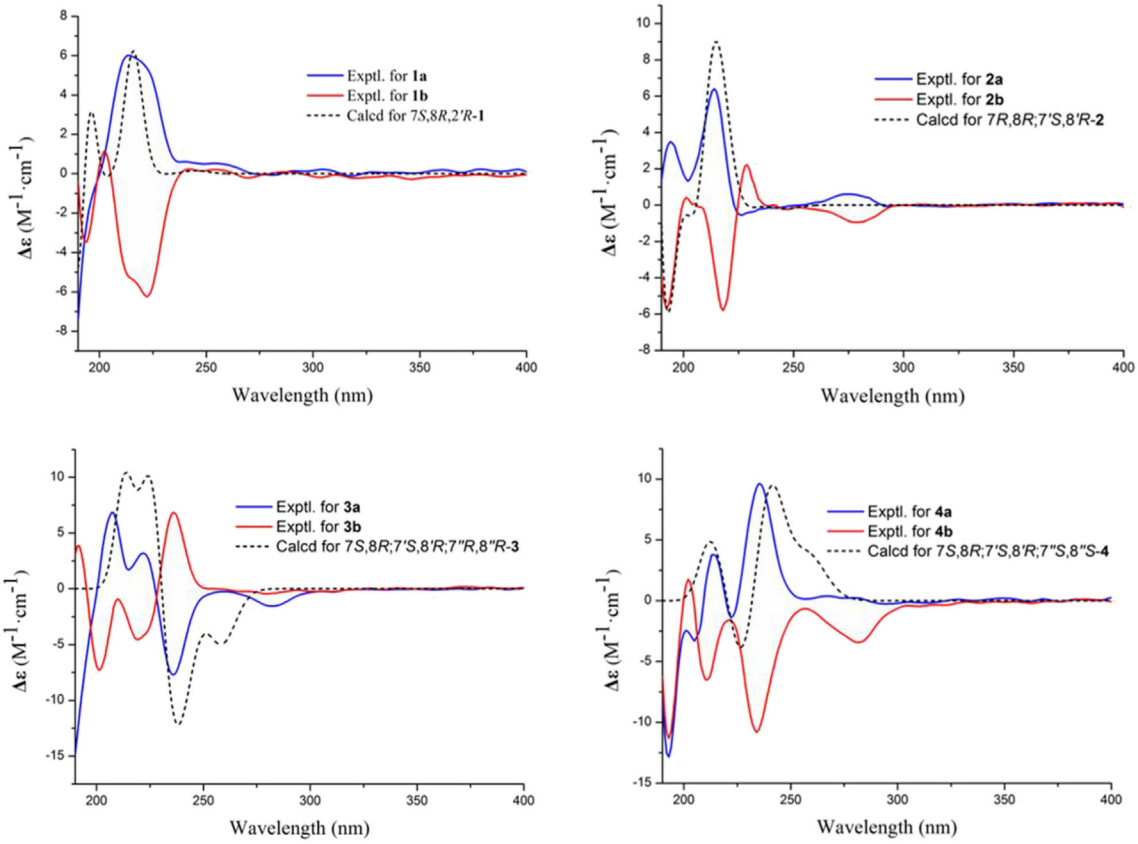

Fig. 4. Calculated and experimental ECD spectra of **1a**/**1b**-**4a**/**4b**.

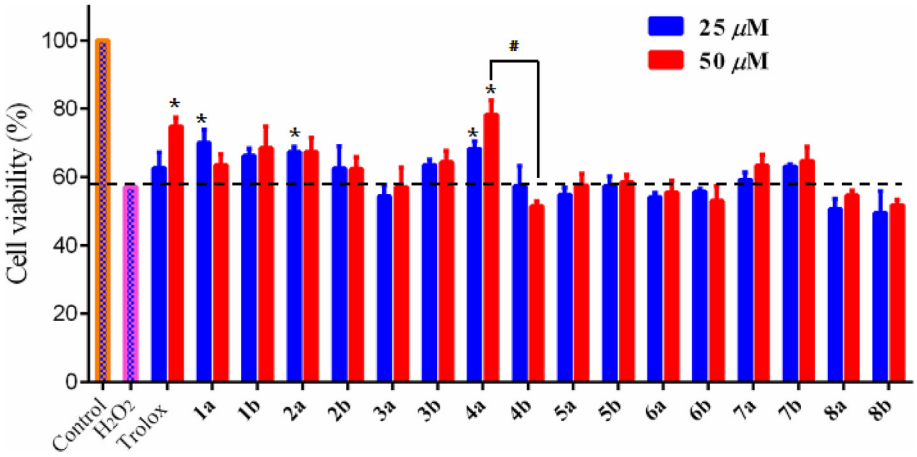

Fig. 5. Neuroprotective effects of compounds against H_2O_2-induced cell growth inhibition of SH-SY5Y cells. In the presence or absence of the tested compounds at different concentrations (25 and 50 μM), MTT assay was used to examine the cell viability after H_2O_2 (300 μM) treatment for 4 h $^{*}P < 0.05$, $^{**}P < 0.01$ vs. H_2O_2-treated group; $^{\#}P < 0.05$ was considered statistically significant when compared with its enantiomer.

chemical diversity and multifarious clinical pharmacology activities (Saleem et al., 2005). The recent decades have witnessed a renewed interest in biologically active lignans isolated from a plethora of natural resources (Teponno et al., 2016; Pan et al., 2009). Currently, the neuroblastoma SH-SY5Y cell line has been widely used to study the molecular and cellular mechanisms underlying the effects of some of the neurodegenerative disorders, although it is not classified as purely dopaminergic neurons cell (Xicoy et al., 2017). All the isolated compounds (**1a**/**1b**-**8a**/**8b**) were evaluated for their neuroprotective effects against H_2O_2-induced oxidative stress in human neuroblastoma SH-SY5Y cells by the MTT assay (Qi et al., 2018). The results (Fig. 5) showed that compounds **1a** and **4a** exhibited significant neuroprotective activity against H_2O_2-induced neurotoxicity at 25 μM concentration, improving cell viability by 13% and 21% compared with the negative control group, respectively. Compounds **1b**, **2a** and **3a** showed weak neuroprotective effects at both 25 and 50 μM concentration. Interestingly, however, compound **4b**, which is the enantiomer of **4a**, showed no effect against H_2O_2-induced neurotoxicity at the concentration of 25 and 50 μM.

To further determine the protective effect of enantiomers **4a** and **4b** on the H_2O_2-treated SH-SY5Y cells, Annexin V/propidium iodide (AV/PI) staining was performed to quantitatively determine the apoptotic cell percentage by flow cytometry. As shown in Fig. 6, after treatment with 25 or 50 μM **4a** for 24 h, the percentages of both early and late apoptotic cells decreased significantly relative to those of the untreated control, while its enantiomer **4b** could not decrease the percent of apoptotic cells induced by H_2O_2.

In general, neuronal cell damage is the most important factor in many neurodegenerative disorders. Epidemiological studies demonstrated that a dietary intake of phenolics have an inverse relationship with the risk of various neuronal cell damage-mediated diseases including Parkinson's disease, Alzheimer's disease, stroke and other neurodegenerative diseases (Chen et al., 2008; Kim et al., 2010; Jan and Ho, 2014). However, clinical evidence regarding the specific role of dietary lignans in the prevention of neurodegenerative diseases is still very limited. It should be noticed that the efficacy of a natural compound in vivo depends on not only its intrinsic bioactivity but also its bioavailability.

According to in vitro studies, when the dietary lignans most commonly found in food are incubated with human fecal microflora, they are transformed to the tetrahydrofuranoid metabolites or enterolignans (Wan et al., 2006; Pan et al., 2005). Besides, the current studied showed that these lignans may be incorporated into the liver and then transported to other tissues (lung, kidney, and brain) via the lymphatic system after oral administration (Jan et al., 2012). The highest concentrations of its conjugated metabolites (glucuronide/sulfate) in liver and kidney suggested that they were regard as the major tissues of metabolism (Tomimori et al., 2017; Valdés et al., 2015).

The blood−brain barrier is a primary interface between the peripheral fluids and the central nervous system, which plays an important role in the brain by preventing potentially neurotoxic plasma components, pathogens, and blood cells from permeating the brain (Zhao et al., 2015). Although limited knowledge is known about the capacity of dietary lignans to cross the blood-brain barrier, relevant researches

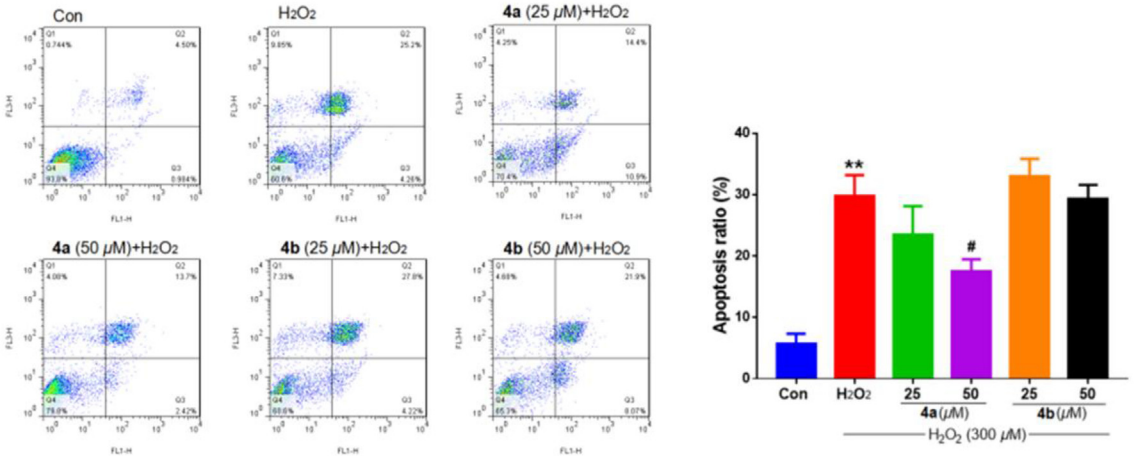

Fig. 6. Effects of **4a** and **4b** on H_2O_2-induced apoptosis in SH-SY5Y cells. Cells were incubated with indicated concentrations of **4a** and **4b** for 12 h before exposure to 300 μM H_2O_2 for 3 h. Representative patterns of flow cytometric distribution of SH-SY5Y cells after Annexin V-PI double staining and the quantitative analysis of apoptotic cells. Data are presented as means ± S.D. (n = 3). $^{\#}p < 0.05$ vs. the control group. $^{**}p < 0.01$ vs. the H_2O_2-treated group.

demonstrated that some furofuran lignans in sesame seeds, such as sesamin and sesamolin, showed varying degrees of potential to migrate across the blood-brain barrier (Liu et al., 2017; Katayama et al., 2016). However, whether these dietary lignans or their derived metabolites produced in vivo could actually enter the brain and play a role in the central nervous system remains unclear. This means that more animal model studies are necessary to determine the metabolism and tissue distribution in the body as well as elucidate the underlying molecular mechanisms for the neuroprotective effects of these polyphenol-derived metabolites.

3. Conclusions

In conclusion, two pairs of enantiomeric furolactones (**1a/1b** and **5a/5b**), four pairs of enantiomeric furofurans (**2a/2b**, **6a/6b**-**8a/8b**) and two pairs of sesquineolignans (**3a/3b** and **4a/4b**), were isolated and identified from 70% aqueous ethanol extract of the fruits of *Rubus idaeus* L. (Rosaceae). These racemic mixtures were successfully separated by HPLC using Daicel chiral-pak IC and AD-H chiral columns with various mobile phases. The structure determination was based on extensive spectroscopic data analyses (NMR, HRESIMS), and the absolute stereochemistry of the undescribed lignans (**1b**, **2a/2b**-**4a/4b**) were determined by comparison between experimental and calculated electronic circular dichroism (ECD) and DP4 plus probability calculations. The isolates were tested for their neuroprotective activity using H_2O_2-treated human neuroblastoma SH-SY5Y cell line. (+)-idaeusinol A (**1a**) and (+)-idaeusinol D (**4a**) exhibited significant neuroprotective activity at 25 μM concentration. Interestingly, however, compound (−)-idaeusinol D (**4b**), which is the enantiomer of **4a**, showed no effect against H_2O_2-induced neuroprotective effect at both 25 and 50 μM concentrations.

4. Experimental

4.1. General experimental procedures

Optical rotations were obtained on a PerkinElmer 341 digital polarimeter. UV and IR spectra were recorded on Shimadzu UV-1700 spectrometer and Bruker IFS-55 spectrometer, respectively. CD spectra were given by Bio-Logic MOS 450 detector. NMR spectra were recorded on Bruker ARX-400 and AV-600 spectrometers. Chemical shifts were presented in δ (ppm) using tetramethylsilane (TMS) as an internal standard, and coupling constants (J) were expressed in Hz. HRESIMS spectra were taken on a Bruker Micro Q-TOF spectrometer (positive-ion mode). High-performance liquid chromatography (HPLC) was performed on a Waters 1525 series pumping system equipped with a Waters 2489 UV–vis detector using an YMC-pack ODS-A column (250 mm × 10 mm, 5 μm) and Waters preparative RP-C_{18} column (19 × 150 mm, 10 μm), and the chiral-pak IC column (250 mm × 4.6 mm, 5 μm) or chiral-pak AD-H column (250 mm × 4.6 mm, 5 μm). Column chromatography was performed on silica gel (100–200 mesh and 200–300 mesh; Qingdao Marine Chemical, Inc., Qingdao, China), octadecyl silica gel (ODS, 60–80 μm, Merck, Darmstadt, Germany), macroporous resin (D101, Cangzhou Baoen Chemistry Ltd, Hebei, China). Thin-layer chromatography (TLC) was carried out on precoated silica gel GF_{254} plates.

4.2. Plant material

The fruits of *Rubus idaeus* L. (Rosaceae) were collected from raspberry planting basement, Dongling district, Shenyang, Liaoning province, PR China (N41°41′9.86″, E123°41′35.24″) in June 2015, and then authenticated by Prof. Jin-Cai Lu, Shenyang Pharmaceutical University, Shenyang, China. A voucher specimen (No. 20150601) has been deposited in the Herbarium of Shenyang Pharmaceutical University for further reference.

4.3. Extraction and isolation

The air-dried fruits of *Rubus idaeus* L. (20 kg) were extracted by maceration in 70% aqueous ethanol (3 × 50 L) at room temperature. The filtrates were concentrated on a rotary evaporator at 45 °C under reduced pressure, which obtained a dark black residue (1.7 kg). The crude extract was then suspended in distilled H_2O and subjected to D101 macroporous resin column eluting with a step gradient solvent system EtOH–H_2O (20:80 → 100:0) to give four fractions (I − IV). Fraction III (176 g) was further submitted to separation over silica gel column using CH_2Cl_2–MeOH (8:1 → 1:2), which resulted in seven subfractions (III_a ~ III_g). Fraction III_b (26.5 g) was separated on a reverse-phase C_{18} silica gel column using gradient elution with aqueous EtOH (20% → 70%), which yielded six pooled subfractions (A − F) on the basis of HPLC analysis. Next, fractions A (4.1 g) was chromatographed on silica gel eluted with CH2Cl2–MeOH (9:1 → 1:1) to afford five subfractions (A1 ~ A5) on the basis of silica gel TLC analysis. Consequently, subfraction A1-1 was further isolated by preparative HPLC on a YMC RP-C_{18} column with MeOH–H_2O (22:78, v/v) as a mobile phase to obtain five fractions (A1-1 ~ A1-5). Then, A1-1 was successively purified by semipreparative HPLC-C_{18} column chromatography with solvent system MeCN–H_2O (10:90, 3.5 mL/min) to yield **1** (17.4 mg) and **7** (6.6 mg). Compound **2** (5.8 mg) was isolated by semipreparative HPLC-C_{18} column chromatography (MeCN–H_2O, 12:88, v/v) from Fr.A1-2. Similarly, fractions B (5.4 g) was chromatographed on silica gel with a gradient of CH_2Cl_2–MeOH system (9:1 → 1:1) as eluents, yielding five fractions (B1 ~ B5). Fr.B4 was separated with preparative HPLC (eluted with MeOH–H_2O, 22:78, v/v) followed by purification with Semipreparative HPLC-C_{18} column chromatography to obtain compounds **5** (8.2 mg), **6** (30.6 mg) and **8** (7.6 mg). In the same manner using preparative HPLC (eluted with MeOH–H_2O, 30:70, v/v), **3** and **4** (22.8 mg) as a mixture were isolated from fraction B3.

Compounds **1**–**8** were further analyzed by HPLC system equipped with different types of analytical chiral columns. Among them, **1** and **5** were subjected to chiral HPLC, respectively, using a Daicel IC column (2-propanol/*n*-hexane, 20:80, v/v, 0.8 mL/min) to afford **1a** (2.5 mg, t_R 21.3 min), **1b** (2.7 mg, t_R 26.5 min), **5a** (1.3 mg, t_R 19.4 min), **5b** (1.1 mg, t_R 28.5 min), respectively. Chiral resolution of **2**, **6**, **7**, **8** were performed on Daicel chiral-pak AD-H column (eluted with 2-propanol/*n*-hexane, 45:55, v/v, flow rate 0.8 mL/min) to give **2a** (1.7 mg, t_R 20.3 min), **2b** (1.9 mg, t_R 34.1 min), **6a** (1.7 mg, t_R 16.5 min), **6b** (1.9 mg, t_R 29.8 min), **7a** (2.7 mg, t_R 25.5 min), **7b** (3.0 mg, t_R 38.8 min), **8a** (3.3 mg, t_R 20.8 min), **8b** (3.2 mg, t_R 29.8 min), respectively. **3** and **4** were obtained together from one peak on the semi-preparative HPLC, and had been divided into four peaks on Daicel chiral-pak IC column (eluted with 2-propanol/*n*-hexane, 20:80, v/v, 0.8 mL/min), subsequently, **3a** and **4b** were further purified by chiral HPLC equipped with Daicel chiral-pak AD-H column eluting with 2-propanol/*n*-hexane (15:85, v/v, 0.6 mL/min), As a result, optically pure compounds of **3a** (1.2 mg, t_R 25.2 min), **3b** (1.1 mg, t_R 128.3 min), **4a** (1.3 mg, t_R 40.8 min), **4b** (1.2 mg, t_R 28.5 min) were successfully achieved.

4.3.1. Idaeusinol A (1)

Pale amorphous gum; $[\alpha]^{20}{}_D$ +0.1 (*c* 0.1, MeOH); UV (MeOH) λ_{max} (log ε) 227 (3.89), 277 (3.10) nm; IR (KBr) ν_{max} 3423, 2924, 1630, 1427, 1006 cm^{-1}; ^1H and ^{13}C NMR (CD_3OD) data, see Table 1; HRESIMS (positive-ion mode) *m/z* 243.0605 $[M + Na]^+$ (calcd for $C_{12}H_{12}O_4Na$, 243.0633).

(+)-*idaeusinol A* (***1a***), pale amorphous gum; $[\alpha]^{20}{}_D$ +24.4 (*c* 0.1, MeOH); ECD (MeOH) 214 ($\Delta\varepsilon$ +6.02) nm; (−)-*idaeusinol A* (***1b***), pale amorphous gum; $[\alpha]^{20}{}_D$ −24.6 (*c* 0.1, MeOH); ECD (MeOH) 222 ($\Delta\varepsilon$ −6.24) nm.

4.3.2. Idaeusinol B (2)

Colorless, light oil; $[\alpha]^{20}_{D}$ −0.3 (*c* 0.1, MeOH); UV (MeOH) λ_{max} (log ε) 226 (4.16), 277 (3.45) nm; IR (KBr) ν_{max} 3417, 2963, 1428, 1266, 1007 cm^{-1}; ^{1}H and ^{13}C NMR (DMSO-d_6) data, see Table 1; HRESIMS (positive-ion mode) *m/z* 321.1085 $[M + Na]^+$ (calcd for $C_{18}H_{18}O_4Na$, 321.1097).

(−)-*idaeusinol B* ***(2a)***, colorless oil; $[\alpha]^{20}_{D}$ −36.3 (*c* 0.14, MeOH); ECD (MeOH) 218 ($\Delta\varepsilon$ −5.81), 229 ($\Delta\varepsilon$ +2.21), 278 ($\Delta\varepsilon$ −0.95) nm; (+)-*idaeusinol B* ***(2b)***, colorless oil; $[\alpha]^{20}_{D}$ +38.1 (*c* 0.14, MeOH); ECD (MeOH) 214 ($\Delta\varepsilon$ +6.41), 226 ($\Delta\varepsilon$ −0.55), 275 ($\Delta\varepsilon$ +0.60) nm.

4.3.3. Idaeusinol C (3)

Light yellow oil; UV (MeOH) λ_{max} (log ε) 228 (3.91), 278 (3.35) nm; IR (KBr) ν_{max} 3480, 1626, 1430, 986 cm^{-1}; ^{1}H and ^{13}C NMR (DMSO-d_6) data, see Table 1; HRESIMS (positive-ion mode) *m/z* 517.1854 $[M + Na]^+$ (calcd for $C_{28}H_{30}O_8Na$, 517.1838).

(+)-*idaeusinol C* ***(3a)***, light yellow oil; $[\alpha]^{20}_{D}$ +31.7 (*c* 0.1, MeOH); ECD (MeOH) 207 ($\Delta\varepsilon$ +6.83), 222 ($\Delta\varepsilon$ +3.19), 237 ($\Delta\varepsilon$ −7.56), 282 ($\Delta\varepsilon$ −1.55) nm; (−)-*idaeusinol C* (**3b**), light yellow oil; $[\alpha]^{20}_{D}$ −30.6 (*c* 0.1, MeOH); ECD (MeOH) 201 ($\Delta\varepsilon$ −7.27), 219 ($\Delta\varepsilon$ −4.54), 236 ($\Delta\varepsilon$ +6.86), 279 ($\Delta\varepsilon$ −0.44) nm.

4.3.4. Idaeusinol D (4)

Light yellow oil; UV (MeOH) λ_{max} (log ε) 228 (3.95), 278 (3.37) nm; IR (KBr) ν_{max} 3422, 2926, 1630, 1426, 1006 cm^{-1}; ^{1}H and ^{13}C NMR (DMSO-d_6) data, see Table 1; HRESIMS (positive-ion mode) *m/z* 517.1854 $[M + Na]^+$ (calcd for $C_{28}H_{30}O_8Na$, 517.1838).

(+)-*idaeusinol D* ***(4a)***, light yellow oil; $[\alpha]^{20}_{D}$ +29.5 (*c* 0.1, MeOH); ECD (MeOH) 211 ($\Delta\varepsilon$ −6.51), 234 ($\Delta\varepsilon$ −10.82), 282 ($\Delta\varepsilon$ −3.42) nm; (−)-*idaeusinol D* ***(4b)***, light yellow oil; $[\alpha]^{20}_{D}$ −28.3 (c 0.1, MeOH); ECD (MeOH) 214 ($\Delta\varepsilon$ +3.78), 235 ($\Delta\varepsilon$ +9.62), 294 ($\Delta\varepsilon$ −0.26) nm.

4.4. ECD and NMR computational details

4.4.1. ECD calculations

Conformational analyses were initially performed using CONFLEX software (Goto and Osawa, 1989) with the using Merck Molecular Force Field (MMFF94) with 10 kcal/mol upper energy limit. Then, the predominant conformers were initially optimized at the quantum mechanical (QM) level using the B3LYP functional and the 6-31G(d,p) basis set. Subsequently, the theoretical calculation of ECD was performed using time dependent Density Functional Theory (TDDFT) at B3LYP/6-311 + G(d,p) level in CH_3OH with PCM model. The ECD spectra of compounds **1a/1b–4a/4b** were obtained by weighing the Boltzmann distribution ratio of each geometric conformation.

4.4.2. NMR calculations

The gauge–including atomic orbital (GIAO) shielding constants of all conformers were calculated after geometry optimization using the B3LYP/6-311 + G(2d,p) level in a methanol solvent model with Gaussian 09 software. The Boltzmann-weighted conformer population was calculated based on the Gibbs free energy from the geometry optimization step. Then, Boltzmann-weighted averages of the chemical shifts were calculated to scale them against the experimental values. The DP4 plus probability was applied to compute the chemical shift errors.

4.5. Cell culture

Human neuroblastoma SH-SY5Y cells (ATCC, Manassas, USA) were cultured in DMEM medium (Hyclone, Logan, USA) supplemented with 10% fetal bovine serum (FBS, Gibco, Gaithersburg, USA) in a humidified atmosphere containing 5% CO_2 at 37 °C. Logarithmically growing cells were used in all the experiments.

4.6. Neuroprotection bioassays

All isolates were evaluated for in vitro neuroprotective activitiy against H_2O_2-induced toxicity in human neuroblastoma cells with the MTT assay. Briefly, SH-SY5Y cells were pretreated with various of concentrations (25 and 50 μM) of tested samples for 1 h before H_2O_2 (300 μM) treatment for another 4 h. Then, 20 μL MTT (5 mg/mL) was added to each well for 4 h, and the crystals were dissolved in DMSO. Optical density at 490 nm was determined by using a plate microreader (Thermo, USA).

4.7. Annexin V-FITC/PI staining

Annexin V-FITC and PI double-staining assay was applied to evaluate apoptotic ratio according the manufacturer's instructions (Azadmehr et al., 2015). The treated cells were stained with Annexin V-FITC followed by PI at room temperature for 15 min. Early and late apoptotic changes in different cells were analyzed by FACScan flow cytometry (Becton Dickinson, USA).

4.8. Statistical analysis

All results and data were confirmed in at least three separate experiments. Data are expressed as means ± SD. Statistical comparisons were analyzed by student's t-test using GraphPad Prism. $P < 0.05$ was considered statistically significant.

Conflicts of interest

The authors declare no conflict of interest.

Acknowledgments

This research was financially supported by Cancer Development Support for Young and Middle-aged Teachers in Shenyang Pharmaceutical University (ZQN2018006) and the Project of Innovation Team (LT2015027) of Liaoning of P. R. China.

Appendix A. Supplementary data

Supplementary data to this article can be found online at https://doi.org/10.1016/j.phytochem.2019.05.008.

References

Azadmehr, A., Hajiaghaee, R., Baradaran, B., Haghdoost-Yazdi, H., 2015. Apoptosis cell death effect of *Scrophularia variegata* on breast cancer cells via mitochondrial intrinsic pathway. Adv. Pharm. Bull. 5, 443–446.

Blumenthal, M., 1998. The Complete Commission German E Monographs: Therapeutic Guide to Herbal Medicines, first ed. American Botanical Council, Texas, USA.

Chen, L.W., Wang, L.Q., Wei, L.C., Shi, M., Chan, Y.S., 2008. Chinese herbs and herbal extracts for neuroprotection of dopamine neurons and potential therapeutic treatment of Parkinson's disease. CNS Neurol. Disord. Drug Targets 6, 273–281.

Chen, M., Xu, X., Xu, B., Yang, P., Liao, Z., Morris-Natschke, S.L., Lee, K.H., Chen, D., 2013. Neglschisandrins E-F: two new lignans and related cytotoxic lignans from *Schisandra neglecta*. Molecules 18, 2297–2306.

Ciric, A., Jelikic-Stankov, M., Cvijovic, M., Djurdjevic, P., 2018. Statistical optimization of an RP-HPLC method for the determination of selected flavonoids in berry juices and evaluation of their antioxidant activities. Biomed. Chromatogr. 32, e4150.

Cuenca, M.D.R., Catalan, C.A.N., Diaz, J.G., Herz, W., 1991. Monoterpenes and lignans from *Mikania saltensis*. J. Nat. Prod. 54, 1162–1164.

Frisch, M.J., Trucks, G.W., Schlegel, H.B., Scuseria, G.E., Robb, M.A., Cheeseman, J.R., Scalmani, G., Barone, V., Mennucci, B., Petersson, G.A., Nakatsuji, H., Caricato, M., Li, X., Hratchian, H.P., Izmaylov, A.F., Bloino, J., Zheng, G., Sonnenberg, J.L., Hada, M., Ehara, M., Toyota, K., Fukuda, R., Hasegawa, J., Ishida, M., Nakajima, T., Honda, Y., Kitao, O., Nakai, H., Vreven, T., Montgomery Jr., J.A., Peralta, J.E., Ogliaro, F., Bearpark, M., Heyd, J.J., Brothers, E., Kudin, K.N., Staroverov, V.N., Kobayashi, R., Normand, J., Raghavachari, K., Rendell, A., Burant, J.C., Iyengar, S.S., Tomasi, J., Cossi, M., Rega, N., Millam, J.M., Klene, M., Knox, J.E., Cross, J.B., Bakken, V., Adamo, C., Jaramillo, J., Gomperts, R., Stratmann, R.E., Yazyev, O., Austin, A.J., Cammi, R., Pomelli, C., Ochterski, J.W., Martin, R.L., Morokuma, K., Zakrzewski, V.G., Voth, G.A., Salvador, P., Dannenberg, J.J., Dapprich, S., Daniels, A.D., Farkas,

Ö., Foresman, J.B., Ortiz, J.V., Cioslowski, J., Fox, D.J., 2009. Gaussian 09, Revision A.02. Gaussian, Inc., Wallingford, CT.
Garcia, G., Nanni, S., Figueira, I., Ivanov, I., Mcdougall, G.J., Stewart, D., Stewart, D., Ferreira, R.B., Pinto, P., Silva, R.F.M., Brites, D., Santos, C.N., 2017. Bioaccessible (poly)phenol metabolites from raspberry protect neural cells from oxidative stress and attenuate microglia activation. Food Chem. 215, 274–283.
Ghalayini, I.F., Al-Ghazo, M.A., Harfeil, M.N., 2011. Prophylaxis and therapeutic effects of raspberry (*Rubus idaeus*) on renal stone formation in Balb/c mice. Int. Braz. J. Urol. 37, 259–267.
González, A.G., Estévez-Reyes, R., Mato, C., 1989. Salicifoliol, a new furolactone-type lignan from *Bupleurum salicifolium*. J. Nat. Prod. 52, 1139–1142.
Goto, H., Osawa, E., 1989. Corner flapping: a simple and fast algorithm for exhaustive generation of ring conformations. J. Am. Chem. Soc. 111, 8950–8951.
Grimblat, N., Zanardi, M.M., Sarotti, A.M., 2015. Beyond DP4: an improved probability for the stereochemical assignment of isomeric compounds using quantum chemical calculations of NMR shifts. J. Org. Chem. 80, 12526–12534.
Hosokawa, A., Sumino, M., Nakamura, T., Yano, S., Sekine, T., Ruangrungsi, N., Watanabe, K., Ikegami, F., 2004. A new lignan from *Balanophora abbreviata* and inhibition of lipopolysaccharide (LPS)-induced inducible nitric oxide synthase (iNOS) expression. Chem. Pharm. Bull. 52, 1265–1267.
Jan, K.C., Ho, C.T., 2014. Inhibitory activity of sesaminol and sesaminol triglycoside on cytochrome P450 enzymes and their pharmacokinetics in rats. J. Funct. Foods 7, 142–149.
Jan, K.C., Chang, Y.W., Hwang, L.S., Ho, C.T., 2012. Tissue distribution and cytochrome P450 inhibition of sesaminol and its tetrahydrofuranoid metabolites. J. Agric. Food Chem. 60, 8616–8623.
Katayama, S., Sugiyama, H., Kushimoto, S., Uchiyama, Y., Hirano, M., Nakamura, S., 2016. Effects of sesaminol feeding on brain Aβ accumulation in a senescence-accelerated mouse-prone 8, SAMP8. J. Agric. Food Chem. 64, 4908–4913.
Kim, J., Lee, H.J., Lee, K.W., 2010. Naturally occurring phytochemicals for the prevention of Alzheimer's disease. J. Neurochem. 112, 1415–1430.
Kim, K.H., Moon, E., Kim, H.K., Oh, J.Y., Kim, S.Y., Choi, S.U., Lee, K.R., 2012. Phenolic constituents from the rhizomes of *Acorus gramineus* and their biological evaluation on antitumor and anti-inflammatory activities. Bioorg. Med. Chem. Lett 22, 6155–6159.
Kobayashi, M., Ohta, Y., 1983. Induction of stress metabolite formation in suspension cultures of *Vigna angularis*. Phytochemistry 22, 1257–1261.
Kumar, M., Rawat, P., Rahuja, N., Srivastava, A.K., Maurya, R., 2009. Antihyperglycemic activity of phenylpropanoyl esters of catechol glycoside and its dimers from *Dodecadenia grandiflora*. Phytochemistry 70, 1448–1455.
Li, W.J., Zhang, Z.H., Cheng, X.L., Liu, J., He, Y., Zhou, C., Guo, Y., Lin, R.C., Wang, G.L., 2012. Two new compounds isolated from *Liriope muscari*. Molecules 17, 8773–8781.
Li, X.N., Chu, C., Tong, S.Q., Cheng, D.P., Yan, J.Z., 2013. A new furolactone-type lignan from *Lycium chinense*. Nat. Prod. Res. 27, 750–752.
Liu, Y.L., Xu, Z.M., Yang, G.Y., Yang, D.X., Ding, J., Chen, H., Yuan, F., Tian, H.L., 2017. Sesamin alleviates blood-brain barrier disruption in mice with experimental traumatic brain injury. Acta Pharm. Sin. https://doi.org/10.1038/aps.2017.103.
Lu, Y.Y., Xue, Y.B., Liu, J.J., Yao, G.M., Li, D.Y., Sun, B., Zhang, J.W., Liu, Y.F., Qi, C.X., Xiang, M., Luo, Z.W., Du, G., Zhang, Y.H., 2015. (±)-Acortatarinowins A–F, norlignan, neolignan, and lignan enantiomers from *Acorus tatarinowii*. J. Nat. Prod. 78, 2205–2214.
Lu, Y.Y., Xue, Y.B., Chen, S.J., Zhu, H.C., Zhang, J.W., Li, X.N., Wang, J.P., Liu, J.J., Qi, C.X., Du, G., Zhang, Y.H., 2016. Antioxidant lignans and neolignans from *Acorus tatarinowii*. Sci. Rep. 6, 22909.
Mazur, W.M., Uehara, M., Wähälä, K., Adlercreutz, H., 2000. Phyto-oestrogen content of berries, and plasma concentrations and urinary excretion of enterolactone after a single strawberry-meal in human subjects. Br. J. Nutr. 83, 381–387.
Mcdougall, G.J., Allwood, J.W., Pereira-Caro, G., Brown, E.M., Latimer, C., Dobson, G., Stewart, D., Ternan, N.G., Lawther, R., O'Connor, G., Rowland, I., Crozier, A., Gill, C.I.R., 2017. The composition of potentially bioactive triterpenoid glycosides in red raspberry is influenced by tissue, extraction procedure and genotype. Food Funct. 8, 3469–3479.
Mei, R.Q., Wang, Y.H., Du, G.H., Liu, G.M., Zhang, L., Cheng, Y.X., 2009. Antioxidant lignans from the fruits of *Broussonetia papyrifera*. J. Nat. Prod. 72, 621–625.
Min, B.S., Na, M.K., Oh, S.R., Ahn, K.S., Jeong, G.S., Li, G., Lee, S.K., Joung, H., Lee, H.K., 2004. New furofuran and butyrolactone lignans with antioxidant activity from the stem bark of *Styrax japonica*. J. Nat. Prod. 67, 1980–1984.
Pan, Q.R., Tao, W., Lu, Q.H., Hu, X., 2005. Schisandrin B, a novel inhibitor of P glycoprotein. Biochem. Biophys. Res. Commun. 335, 406–411.
Pan, J.Y., Chen, S.L., Yang, M.H., Wu, J., Sinkkonen, J., Zoud, K., 2009. An update on lignans: natural products and synthesis. Nat. Prod. Rep. 26, 1251–1292.
Qi, X.L., Zhang, Y.Y., Zhao, P., Zhou, L., Wang, X.B., Huang, X.X., Lin, B., Song, S.J., 2018. ent-Kaurane diterpenoids with neuroprotective properties from corn silk (*Zea mays*). J. Nat. Prod. 81, 1225–1234.
Rao, A.V., Snyder, D.M., 2010. Raspberries and human health: a review. J. Agric. Food Chem. 58, 3871–3883.
Saleem, M., Kim, H.J., Ali, M.S., Lee, Y.S., 2005. An update on bioactive plant lignans. Nat. Prod. Rep. 22, 696–716.
Shao, S.Y., Yang, Y.N., Feng, Z.M., Jiang, J.S., Zhang, P.C., 2018. An efficient method for determining the relative configuration of furofuran lignans by ^{1}H NMR spectroscopy. J. Nat. Prod. 81, 1023–1028.
Teponno, R.B., Kusari, S., Spiteller, M., 2016. Recent advances in research on lignans and neolignans. Nat. Prod. Rep. 33, 1044–1092.
Tomimori, N., Rogi, T., Shibata, H., 2017. Absorption, distribution, metabolism and excretion of [^{14}C] sesamin in rats. Mol. Nutr. Food Res. 61, 1600844.
Valdés, L., Cuervo, A., Salazar, N., Ruas-Madiedo, P., Gueimonde, M., González, S., 2015. The relationship between phenolic compounds from diet and microbiota: impact on human health. Food Funct. 6, 2424–2439.
Wan, C.K., Zhu, G.Y., Shen, X.L., Chattopadhyay, A., Dey, S., Fong, W.F., 2006. Gomisin A alters substrate interaction and reverses Pglycoprotein-mediated multidrug resistance in HepG2-DR cells. Biochem. Pharmacol. 72, 824–837.
Wang, X.W., Zhang, H.P., Chen, F., Wang, X., Wen, W.Y., 2009. A new lignan from *Gynostemma pentaphyllum*. Chin. Chem. Lett. 20, 589–591.
Xicoy, H., Wieringa, B., Martens, G.J.M., 2017. The SH-SY5Y cell line in Parkinson's disease research: a systematic review. Mol. Neurodegener. 12, 10.
Xiong, L., Zhu, C., Li, Y., Tian, Y., Lin, S., Yuan, S., Hu, J., Hou, Q., Chen, N., Yang, Y., Shi, J., 2011. Lignans and neolignans from Sinocalamus affinis and their absolute configurations. J. Nat. Prod. 74, 1188–1200.
Xue, Y.B., Li, X.F., Du, X., Li, X.N., Wang, W.G., Yang, J.H., Chen, J.J., Pu, J.X., Sun, H.D., 2015. Isolation and anti-hepatitis B virus activity of dibenzocyclooctadiene lignans from the fruits of *Schisandra chinensis*. Phytochemistry 116, 253–261.
Yamauchi, S., Ina, T., Kirikihira, T., Masuda, T., 2004. Synthesis and antioxidant activity of oxygenated furofuran lignans. Biosci. Biotechnol. Biochem. 68, 183–192.
Zhao, Z., Nelson, A.R., Betsholtz, C., Zlokovic, B.V., 2015. Establishment and dysfunction of the blood-brain barrier. Cell 163, 1064–1078.